December 2003 • NREL/TP-500-34478

Technical Report

Semi-Empirical Aeroacoustic Noise Prediction Code for Wind Turbines

P. Moriarty and P. Migliore

National Renewable Energy Laboratory

1617 Cole Boulevard
Golden, Colorado 80401-3393

NREL is a U.S. Department of Energy Laboratory
Operated by Midwest Research Institute • Battelle

Contract No. DE-AC36-99-GO10337

December 2003 • NREL/TP-500-34478

Semi-Empirical Aeroacoustic Noise Prediction Code for Wind Turbines

P. Moriarty and P. Migliore

Prepared under Task No. WER3.1830

National Renewable Energy Laboratory

1617 Cole Boulevard
Golden, Colorado 80401-3393

NREL is a U.S. Department of Energy Laboratory
Operated by Midwest Research Institute • Battelle

Contract No. DE-AC36-99-GO10337

NOTICE

Available electronically at http://www.osti.gov/bridge

Available for a processing fee to U.S. Department of Energy and its contractors, in paper, from:

U.S. Department of Energy
Office of Scientific and Technical Information
P.O. Box 62
Oak Ridge, TN 37831-0062
phone: 865.576.8401
fax: 865.576.5728
email: reports@adonis.osti.gov

Available for sale to the public, in paper, from:

U.S. Department of Commerce
National Technical Information Service
5285 Port Royal Road
Springfield, VA 22161
phone: 800.553.6847
fax: 703.605.6900
email: orders@ntis.fedworld.gov
online ordering: http://www.ntis.gov/ordering.htm


Printed on paper containing at least 50% wastepaper, including 20% postconsumer waste

Foreword

The U.S. Department of Energy (DOE), working through its National Renewable Energy Laboratory (NREL), is engaged in a comprehensive research effort to improve the understanding of wind turbine aeroacoustics. Motivation for this effort is the desire to exploit the large expanse of low wind speed sites that tend to be closer to U.S. load centers. Quiet wind turbines are an inducement to widespread deployment, so the goal of NREL's aeroacoustic research is to develop tools for use by U.S. industry in developing and deploying highly efficient, quiet wind turbines at these low wind speed sites. NREL's National Wind Technology Center (NWTC) is implementing a multifaceted approach that includes wind tunnel tests, field tests, and theoretical analyses in direct support of low wind speed turbine development by its industry partners. NWTC researchers are working hand in hand with industry engineers to ensure that research findings are available to support ongoing design decisions.

This report describes the development and validation of a semi-empirical code for predicting wind turbine aeroacoustic emissions and the resulting sound pressure level at a receptor location. To our knowledge, it is the only such method currently available to U.S. wind turbine designers. The semi-empirical approach has its shortcomings, but improvements are already in the works. Other aspects of our research program, including wind tunnel tests, field tests and computational analysis, will contribute to these improvements. Thus, the present work needs to be considered in the context of the broader research effort on wind turbine aeroacoustics.

Wind tunnel *aerodynamic* tests and *aeroacoustic* tests have been performed on six airfoils that are candidates for use on small wind turbines. Results are documented in the following two companion NREL reports:

> "Wind Tunnel Aeroacoustic Tests of Six Airfoils for Use on Small Wind Turbines,"
> Stefan Oerlemans, Principal Investigator, the Netherlands National Aerospace Laboratory
>
> "Wind Tunnel Aerodynamic Tests of Six Airfoils for Use on Small Wind Turbines,"
> Michael Selig, Principal Investigator, University of Illinois at Urbana-Champaign (UIUC).

These reports provide a valuable airfoil database for designers who wish to consider the tested airfoils. But inevitably, they will wish to evaluate other airfoils that have not been tested. This presents a dilemma. Not only are wind tunnel tests expensive, it is often difficult to schedule the required facilities within the overall timeframe of a project development plan. This conundrum begs the question, "Is it really necessary to conduct wind tunnel tests, or can we rely on theoretical predictions?" Predicting the aeroacoustic emission spectra of a particular airfoil shape is extremely difficult, but predicting the aerodynamic characteristics of a particular airfoil shape is a routine, well-established practice. Nevertheless, there is always some uncertainty about the accuracy of the predictions compared to wind tunnel tests or field performance, and there are questions about the efficacy of the two principal airfoil analysis methods: the Eppler and XFOIL codes. To address these related issues, at least in part, a theoretical analysis was commissioned of the same airfoils tested in the wind tunnel. The results are documented in the following NREL report:

> "Theoretical Aerodynamic Analyses of Six Airfoils for Use on Small Wind Turbines Using Eppler and XFOIL Codes," Dan M. Somers and Mark D. Maughmer; Principal Investigators; Airfoils, Incorporated

The possession of both theoretically predicted aerodynamic characteristics and wind tunnel test data for the same six airfoils provides the extraordinary opportunity to compare the performance, measured by energy capture, of wind turbine rotors designed with the different data. This will provide the desired insight to assist designers in deciding whether to pursue wind tunnel tests. Although some differences in the resulting blade planforms (chord and twist distributions) can be expected, a more important question relates to the difference in energy capture and its significance in driving the choices that need to be made during the preliminary design stage. These issues are addressed in a report that compares the differences in Eppler and XFOIL predictions to the UIUC wind tunnel tests and examines the planform and energy capture differences in resulting blade designs. This report is titled:

> "Comparison of Optimized Aerodynamic Performance of Small Wind Turbine Rotors Designed with Theoretically Predicted versus Experimentally Measured Airfoil Characteristics,"
> Michael Selig, Principal Investigator, University of Illinois at Urbana-Champaign (UIUC)

Another research effort undertaken in support of the U.S. wind turbine industry involves a series of aeroacoustic field tests conducted at the NWTC. Using well documented, consistently applied test procedures, noise spectra were measured for eight small wind turbine configurations. Test results provide valuable information to the manufacturers, as well as the potential users of these turbines. To our knowledge, this is the first comprehensive database of noise data for small wind turbines. Results of this effort are documented in another NREL report, titled:

> "Aeroacoustic Field Tests of Eight Small Wind Turbines," J. van Dam and A. Huskey, Principal Investigators, NREL's National Wind Technology Center

Wind tunnel tests, field tests and theoretical analyses provide useful information for the development and validation of NREL's semi-empirical noise prediction code. This effort, which is described in the following report, will be continuously improved, but may ultimately give way to more sophisticated, physics-based computational aeroacoustic codes also being developed by NREL.

> "Semi-Empirical Aeroacoustic Noise Prediction Code for Wind Turbines," Patrick Moriarty, Principal Investigator, NREL's National Wind Technology Center.

Each of the documents described above will be published as a stand-alone NREL report. Undoubtedly, some results will also be presented in various journal articles or conference papers. All of the NREL reports will be available on NREL's NWTC Web site at http://www.nrel.gov/wind/. Collectively, these reports represent a significant compendium of information on the aerodynamics and aeroacoustics of contemporary wind turbines. Therefore, NREL will also publish a CD-ROM containing all of the reports.

Clearly, this work represents a significant commitment of DOE resources as well as a significant human commitment over an extended period of time. I am sure I express the sentiments of all the research participants in saying we sincerely hope the results of these efforts prove beneficial to the wind energy community.

Paul G. Migliore
NREL/NWTC Project Manager

Table of Contents

Abstract

A series of semi-empirical aeroacoustic noise prediction subroutines was written and incorporated into the National Renewable Energy Laboratory's (NREL's) aeroelastic simulation code: FAST [1]. The subroutines predict six different forms of aerodynamically produced noise that were superimposed to calculate the total aeroacoustic signature of an operating wind turbine. The outputs of the code are sound pressure level spectra of these various sources in one-third octave bands. Parts of the code were validated against acoustic data from two-dimensional airfoil tests. Results from these validation studies were somewhat mixed. For certain wind tunnel conditions, the code predicted sound pressure levels within 2 decibels (dB) of the data, while for others the difference between prediction and data was 6 dB or more. Trends and relative amplitude changes in the predictions often mimicked those seen in the data. Predictions of the NACA 0012 airfoil were more accurate than those of the other airfoils. The code was also validated against measurements from a test of a full-scale wind turbine, the Atlantic Orient Corporation (AOC) 15/50. The noise predictions of this turbine were dominated by turbulent inflow noise, which was found to be sensitive to turbulence intensity and the turbulent length scale. It is unclear whether this dominance of turbulent inflow noise is physically realistic because previous studies have shown this was not the dominant source for wind turbines. Further study of turbulent inflow noise is recommended. Trends in the predicted sound pressure level as a function of wind speed and also the acoustic noise spectrum matched those of the data, although the absolute levels were slightly different. Several parametric studies were performed using the AOC model. It was verified that the total sound pressure level was most sensitive to the rotor's rotational speed. Because of directivity effects, the position of the observer relative to the rotor plane greatly affected the perceived total sound pressure level and also the apparent source distribution across the rotor plane.

Semi-Empirical Aeroacoustic Noise Prediction Code for Wind Turbines

Introduction

One of the most significant drivers for wind turbine design is the amount of acoustic noise that a turbine radiates. This issue is particularly important because turbines are placed closer to load centers, which typically have large population densities and restrictive noise ordinances. To date, the rotational speeds of most wind turbine designs have been limited by the acoustic emissions from the blades, for which the sound intensity is approximately proportional to the tip speed raised to the fifth power. Unfortunately, tip speed is also related to the cost effectiveness of the wind turbine design. Increasing the tip speed, even slightly, can have a dramatic effect on the amount of energy captured by a wind turbine and, hence, directly influences the cost of energy for a given design. Therefore, it is very important to be able to understand, model, and predict the aeroacoustic noise for a given turbine in the design process and to make design changes before prototypes are built and tested. The noise prediction subroutines written to interface with FAST [1] allow these predictions to be made. This report explains how the code was written, what validation against test data was performed, and how a user can implement the code to predict noise for any given turbine design.

Aeroacoustic Noise Prediction Model

The model developed for the prediction of aeroacoustic noise is based on six different noise sources that are assumed to independently generate their own noise signature. The assumption of independence is founded on the idea that the mechanisms for each noise source are fundamentally different from each other or occur in different locations along a turbine blade, such that they do not interfere with one another. These independent noise sources are superimposed to obtain the total noise spectra emitted from the wind turbine rotor. Five of these models are taken directly from the work of Brooks, Pope, and Marcolini [2], who formulated semi-empirical relations for the following sources of noise: turbulent boundary layer trailing edge, separating flow, laminar boundary layer vortex shedding, trailing edge bluntness vortex shedding, and tip vortex formation. These models are based on two-dimensional wind tunnel measurements (except for the tip vortex formation noise) of NACA 0012 airfoils. These noise sources, termed airfoil self-noise, are caused by the interaction between an airfoil and the turbulence produced in its own boundary layer and near wake when encountering a non-turbulent inflow. The final noise source, turbulent inflow noise, is caused by the interaction of the leading edge of the airfoil with a turbulent inflow. The model for this noise source was taken from the works of Lowson [3], who modified equations written by Amiet [4] to apply to wind turbine applications.

Each semi-empirical model relates the properties of the flowfield and turbine geometry to a resulting sound pressure level (SPL). The SPL, given in units of dB, is proportional to the logarithm of the ratio of sound intensity (or mean square pressure) to a reference value:

$$SPL = 10\log\left(\frac{I}{I_{ref}}\right) = 20\log\left(\frac{p}{p_{ref}}\right) \quad [1]$$

where I is the sound intensity, and p is the root mean square sound pressure. The reference root mean square pressure is 20 μPa.

Each of the semi-empirical models was developed for a single two-dimensional airfoil. In order to calculate the aerodynamic noise radiating from a wind turbine rotor, the rotor blades are first discretized into many individual segments. Using local flow velocities and angles of attack, the sound pressure level for each segment and noise source is then calculated relative to an observer position. Finally, the sound pressure level from each of the individual sources is summed across the blade to calculate the total noise signature of the rotor. For the semi-empirical models to be applicable, the segments are assumed to operate in predominantly two-dimensional flow. This is largely true for outboard blade sections, which tend to dominate the noise production. The flow over the segments is also assumed to be quasi-steady, such that the mechanisms that produce noise are stationary at each time step in the simulation.

Turbulent Boundary Layer Trailing Edge (TBL-TE)

The first, and perhaps most common, source of noise from an airfoil, results from the interaction between the turbulent boundary layer and the trailing edge of the airfoil, especially at higher Reynolds numbers. Based on their measurements, Brooks, Pope, and Marcolini formulated empirical relations to predict these noise sources based on the edge-scatter formulation of Ffowcs-Williams and Hall [5]. These relations account for the noise intensity being directly proportional to the turbulent boundary layer displacement thickness, δ^*, and the fifth power of the mean velocity or Mach number, M^5, and inversely proportional to the square of the distance between the observer and the airfoil trailing edge. There are also corrections for angle of attack and Reynolds number, as well as tripped and untripped boundary layers. Turbulent boundary layer noise can originate on both the suction and pressure side of the airfoil. For the pressure side of the airfoil, the sound pressure level is given as follows:

$$SPL_p = 10\log\left(\frac{\delta_p^* M^5 L\overline{D}_h}{r_e^2}\right) + A\left(\frac{St_p}{St_1}\right) + (K_1 - 3) + \Delta K_1 \quad [2]$$

where $\delta^* = \delta^*(\alpha, Re_c)$ is the boundary layer displacement thickness, in meters [m], based on α, the angle of attack [deg.], and Re_c, the Reynolds number based on chord. The subscript p refers to the pressure side of the airfoil. Other parameters in Equation 2 are L, the span of the airfoil section [m]; D_h, the directivity function (see directivity section starting on page 6); r_e, the effective observer distance [m]; and A, an empirical spectral shape based on the Strouhal number $St = (f\delta^*/U)$, where f is the frequency in hertz [Hz], and U is the local mean velocity [m/s]. Three other empirical relations are also used, $St_1 = 0.02M^{-0.6}$, $K_1 = K_1(Re_c)$, and $\Delta K_1 = \Delta K_1(\alpha, Re_{\delta^*})$.

A nearly identical formulation is used to calculate the sound pressure level radiating from the suction side of the airfoil [2].

Separated Flow

As the angle of attack increases from moderate to high, the size of the turbulent boundary layer on the suction side of the airfoil increases dramatically, and large-scale unsteady structures form. These structures can dominate noise production from the trailing edge. When the airfoil is fully separated or stalled, noise radiates from the unsteady flow over the entire chord of the airfoil. This is an important noise source for wind turbines because the blades operate at high angles of attack for significant portions of time. The empirical relation for separated flow noise, denoted SPL_α, is very similar to Equation 2 with different scaling functions for the angle of attack dependence [2].

The total sound pressure level from the interaction of the turbulent boundary layer with the trailing edge can be determined through simple summation of the three different components: pressure side, suction side, and separated flow:

$$SPL_{TBL-TE} = 10\log\left(10^{SPL_p/10} + 10^{SPL_s/10} + 10^{SPL_\alpha/10}\right) \quad [3]$$

Laminar Boundary Layer Vortex Shedding (LBL-VS)

Another source of airfoil self noise [2] is that of laminar boundary layer vortex shedding. The noise from this source is created by a feedback loop between vortices being shed at the trailing edge and instability waves (Tollmien-Schlicting waves [6]) in the laminar boundary layer upstream of the trailing edge. As a laminar vortex leaves the trailing edge, its pressure waves propagate upstream and amplify instabilities in the boundary layer. When these instabilities reach the trailing edge, vortices with similar frequency content are created, forming a feedback loop. This source of noise is most likely to occur on the pressure side of the airfoil and is somewhat tonal in nature because of feedback amplification. This noise source is probably not significant for current utility-sized turbines because their blade airfoil sections, particularly near the tips, operate at fairly large Reynolds number (>1 million), but may be important for smaller sized turbines (i.e. <500 kW). The empirical relation for sound pressure level is as follows:

$$SPL_{LBL-VS} = 10\log\left(\frac{\delta_p M^5 L\overline{D}_h}{r_e^2}\right) + G_1\left(\frac{St'}{St'_{peak}}\right) + G_2\left(\frac{\mathrm{Re}_c}{(\mathrm{Re}_c)_o}\right) + G_3(\alpha) \quad [4]$$

where most of the variables are identical to those in Equation 2: δ_p is the boundary layer thickness [m] on the pressure side of the airfoil; *G1*, *G2*, and *G3* are empirical functions; St' is the Strouhal number based on δ_p, $St'_{peak} = St'_{peak}(Re_c)$ and is the peak Strouhal number; and $(Re_c)_o = (Re_c)_o(\alpha)$ is a reference Reynolds number.

Trailing-Edge Bluntness Vortex Shedding (TEB-VS)

Another source of airfoil self noise is vortex shedding from a blunt trailing edge. The frequency and amplitude of this noise source are largely determined by the geometry of the trailing edge. The vortices shed are typically coherent in nature and can produce discrete tones similar to a Von Karman vortex street downstream of cylindrical objects. This noise source will dominate the total radiated noise if the thickness of the trailing edge is significantly larger than the thickness of

the boundary layer at the trailing edge. Therefore, in addition to Mach number and boundary layer thickness scaling, the empirical relation to predict sound pressure level also contains functions dependent on the trailing edge thickness, as follows:

$$SPL_{TEB-VS} = 10\log\left(\frac{\delta_p^* M^5 L \overline{D}_h}{r_e^2}\right) + G_4\left(\frac{h}{\delta_{avg}^*}, \Psi\right) + G_5\left(\frac{h}{\delta_{avg}^*}, \Psi, \frac{St''}{St''_{peak}}\right) \quad [5]$$

where h is the trailing edge thickness [m]; δ^*_{avg} is the average displacement thickness for both sides of the airfoil [m]; Ψ is the solid angle between both airfoil surfaces just upstream of the trailing edge [deg.]; St'' is the Strouhal number based on h; $St''_{peak} = St''_{peak}(h/\delta^*_{avg})$ is the peak Strouhal number; and G_4 and G are empirical functions of these parameters.

Tip Vortex Formation

The interaction of the tip vortex with the blade tip and trailing edge near the tip is also a source of aerodynamic noise. This noise source is different from the previous four sources in that it is three-dimensional in nature. The sound pressure level is a function of the vortex strength, which is dependent on the spanwise loading on the turbine blade. Typically, the sound pressure levels from tip noise are less than those of trailing edge noise, but tip noise can add significant amounts of noise at higher frequencies. Brooks, Pope, and Marcolini formulated the following relation for an untwisted, constant chord blade:

$$SPL_{Tip} = 10\log\left(\frac{M^2 M_{\max}^5 \ell^2 \overline{D}_h}{r_e^2}\right) - 30.5(\log St'''+0.3)^2 + 126 \quad [6]$$

where $M_{max} = M_{max}(\alpha_{tip})$ is the maximum Mach number within the separated flow region near the tip, α_{tip} is the equivalent angle of attack at the tip [deg.], and $\ell = \ell(\alpha_{tip})$ is the spanwise extent of the separation zone [m], which is dependent on the spanwise lift distribution and the geometric shape of the tip (rounded or square). St''' is the Strouhal number based on ℓ. Because this relation was formulated for an untwisted, constant chord blade, an equivalent α_{tip} for twisted and tapered blades should be used to produce reliable results. A crude estimate for this parameter can be made by multiplying the geometric α_{tip} by the ratio of the slopes of the spanwise lift distribution for the complex blade shape to that of Brooks, Pope, and Marcolini. If accurate estimates of absolute tip noise were necessary, the user would be required to tune this variable to match measured data, which are not easily obtained.

Turbulent Inflow

For wind-turbine applications, the interaction of the turbulent inflow (produced by the atmospheric boundary layer) with the leading edge of the turbine blades is a significant source of noise, particularly at low frequencies. This noise source becomes important when the length scale of the turbulent eddies is large in comparison to the leading edge radius of an airfoil. In the atmospheric boundary layer, the scales of turbulence vary by several orders of magnitude from approximately 1 mm to larger scales on the order of 100 m, where most of the energy resides.

Depending on the size of the length scale relative to the leading edge radius of the airfoil, turbulent inflow can create either a dipole noise source (low-frequency) with M^6 dependence or a scattered quadrupole noise source (high frequency) with M^5 dependence [7]. Lowson [3] formulated an empirical relation for inflow turbulence noise that modeled both the low and high frequency behavior and is based on Amiet's [4] work on experimental airfoil measurements, as follows:

$$SPL_{Inflow} = SPL^{H}_{Inflow} + 10\log\left(\frac{LFC}{1+LFC}\right) \quad [7]$$

$$SPL^{H}_{Inflow} = 10\log\left(\frac{\rho_o^2 c_o^2 lL}{2r_e^2} M^3 u^2 I^2 \frac{K^3}{(1+K^2)^{7/3}} \overline{D}_L\right) + 58.4 \quad [8]$$

$$LFC = 10S^2 MK^2 \beta^{-2} \quad [9]$$

$$S^2 = \left(\frac{2\pi K}{\beta^2} + \left(1 + 2.4\frac{K}{\beta^2}\right)^{-1}\right)^{-1} \quad [10]$$

where ρ_o is the air density [kg/m^3]; c_o is the speed of sound [m/s]; l is a turbulence length scale (described in the next paragraph) [m]; u is the mean wind speed [m/s]; I is the turbulence intensity [%]; $K = \pi fc/U$ is the local wave number, where f is the frequency of interest [Hz], c is the local airfoil chord length [m], and U is the local velocity over the airfoil section [m/s]; D_L is a low-frequency directivity function; LFC is a low-frequency correction factor; S is the compressible Sears function; and $\beta^2 = 1-M^2$.

Note that the sound intensity (the term in brackets in Eq. 8) is directly proportional to the turbulence length scale. Therefore, this parameter should be chosen with care because it will be sensitive to both the rotor size and the nature of the turbulence at the turbine site. Currently, in the code, the isotropic turbulence integral-scale parameter of the atmospheric boundary layer is used, which is a function of the hub height of the turbine, as specified in the International Electrotechnical Commission (IEC) standard [8]. This parameter is defined as 2.45 times the hub height, up to a maximum of 73.5m (30 m hub height). It should be noted for potential users of the code that the turbulent length scale is currently fixed at the IEC value inside the code, although future revisions may include this as an input value.

Tower Wake Interaction

Currently, the prediction code does not model the noise created by blades passing through the wake of the tower, either upwind or downwind. This noise source is a significant contributor for downwind turbines and may be modeled in the future.

Atmospheric Propagation

Currently, the prediction code does not model the effects of the atmosphere or terrain on the propagating noise. These effects include reflections off uneven terrain or buildings, atmospheric

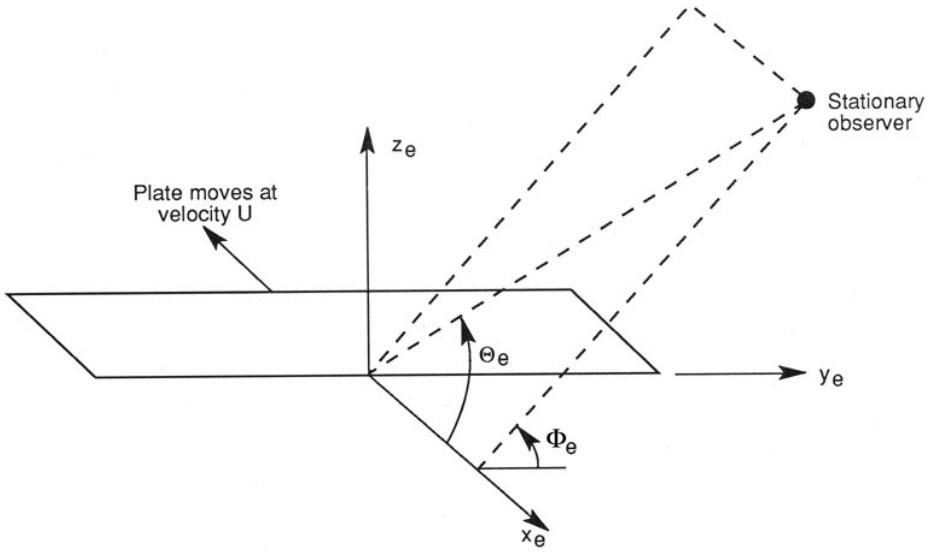

Figure 1. Angles used in directivity functions [2]

absorption, and various modifications caused by propagation through the atmospheric boundary layer. These effects are important for noise propagation over long distances and may be modeled in the future.

Directivity

In each of the empirical relations above, there are correction factors for the directivity of the noise based on the position of the observer relative to either the trailing or leading edge of the airfoil. These correction factors and the noise levels themselves are based on a coordinate system that is shifted or "retarded" relative to the original airfoil positions. This retarded coordinate system compensates for the fact that the noise is convected downstream as it approaches the observer. Source convection changes the apparent location of the noise source and also the relative directivity angles for the observer. In the semi-empirical code, all sources are assumed to convect in the direction of the mean wind speed at a velocity of 0.8 times the mean wind speed, which is approximately the average velocity for an atmospheric boundary layer profile with a power exponent of 0.2.

Once the position of the noise source is determined in retarded coordinates, the directivity angles are determined (Figure 1). Note that all noise sources except for turbulent inflow noise are assumed to originate at the trailing edge of the airfoil, while the turbulent inflow noise originates at the leading edge of the airfoil. These directivity angles are then used in the following directivity functions, which account for some Doppler shift effects and convective amplification of a non-stationary noise source relative to the observer. For high-frequency noise sources (everything except for high-angle separation and turbulent inflow noise) the directivity function is as follows:

$$\overline{D}_H(\Theta_e,\Phi_e) \approx \frac{2\sin^2(\tfrac{1}{2}\Theta_e)\sin^2\Phi_e}{(1+M\cos\Theta_e)\left(1+(M-M_c)\cos\Theta_e\right)^2} \qquad [11]$$

where M is the Mach number for the airfoil section, M_c is the convective Mach number, Θ_e and Φ_e are the directivity angles.

For low-frequency noise sources, the directivity correction is as follows:

$$\overline{D}_L(\Theta_e, \Phi_e) \approx \frac{\sin^2 \Theta_e \sin^2 \Phi_e}{(1 + M \cos \Theta_e)^4} \quad [12]$$

Note that for $\Theta_e = 90°$ and $\Phi_e = 90°$, both directivity functions are equal to 1. Also, D_H becomes increasingly inaccurate for shallow upstream angles, where Θ_e approaches 180°.

Code Validation

To assess the accuracy of the semi-empirical code for absolute and relative values of sound pressure level, researchers compared predicted values to measured data from two-dimensional airfoil tests and measurements of a full-scale wind turbine. They also performed parametric studies of various quantities to determine various sensitivities of the prediction code.

Two-Dimensional Airfoil Data

The first part of code validation involved comparing values predicted by the noise code to two-dimensional airfoil data. The two-dimensional airfoil data were taken from a series of wind-tunnel tests performed at the National Aerospace Laboratory in the Netherlands (NLR) [9]. Acoustic noise spectra of several different airfoils were measured using a 48-microphone acoustic array. Details of the array, array processing, and measurements can be found in [9]. Readers of this report should consider the correction scheme used to eliminate extraneous noise sources from some of the data used in the present study. It should also be noted that using microphone array measurements to calculate absolute sound pressure levels is more computationally complex than measurements from a single microphone, but the technique has been shown to be experimentally valid [10]. Analysis of the acoustic array data provided third-octave sound pressure level measurements that could be directly compared to predictions given by the semi-empirical code. From this data set, two airfoils, a NACA 0012 and an S822 [11], were modeled for code validation. The chord lengths of both airfoils were 0.2286 m.

Figure 2 shows the comparison between data and predictions for a NACA 0012 airfoil at a Mach number of 0.207 for a range of angles of attack. In each of the following figures, the points with symbols represent the measured wind-tunnel data, while the lines of similar color represent the predicted spectra for the same wind conditions. In Figure 2, the assumptions used for the prediction code are that turbulent boundary-layer trailing-edge noise (including separating flow noise) is the dominant source, the boundary layer is "lightly" tripped (see boundary-layer tripping section below), and there is no noise from laminar vortex shedding, trailing edge bluntness, or turbulent inflow (test section turbulence intensity ~0.5%). Because the semi-empirical relations in the prediction code are based on previous measurements of a NACA 0012 airfoil, one would expect that agreement between data and prediction to be fairly close. This is

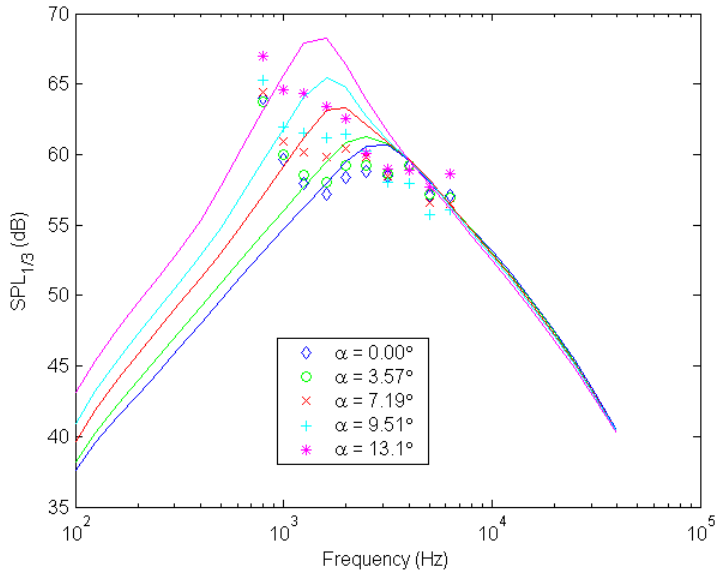

Figure 2. Comparison of two-dimensional NACA 0012 data to predictions for M = 0.207 at several angles of attack

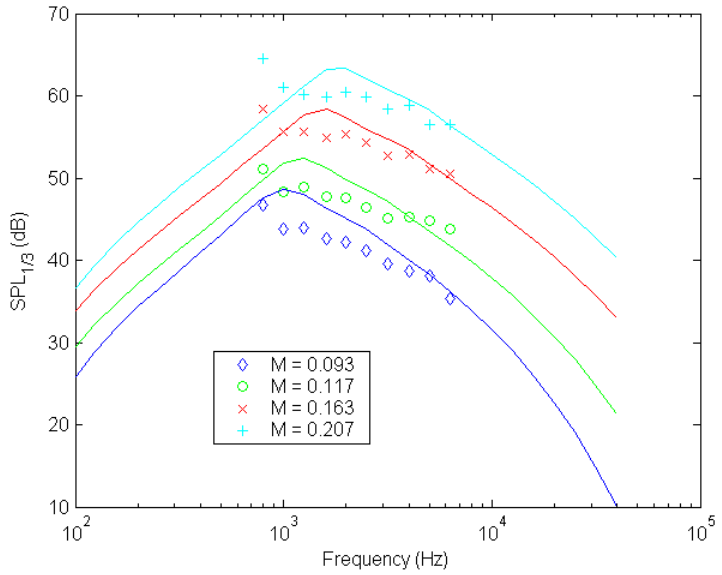

Figure 3. Comparison of two-dimensional NACA 0012 data to predictions for α = 7.18° at several Mach numbers

true for frequencies near 3 kilohertz (kHz), but less so for lower frequencies where the difference is as large as 6 dB. At lower frequencies, the absolute sound pressure levels are overpredicted, but the relative trends and differences in level as a function of angle of attack are very similar to the data. However, the agreement between measurement and prediction worsens with increasing angle of attack.

Figure 3 compares test data and predictions for a NACA 0012 airfoil at an angle of attack of 7.18° and a range of Mach numbers. These tunnel speeds were chosen so that a direct comparison to the measurements of Brooks, Pope, and Marcolini [2]

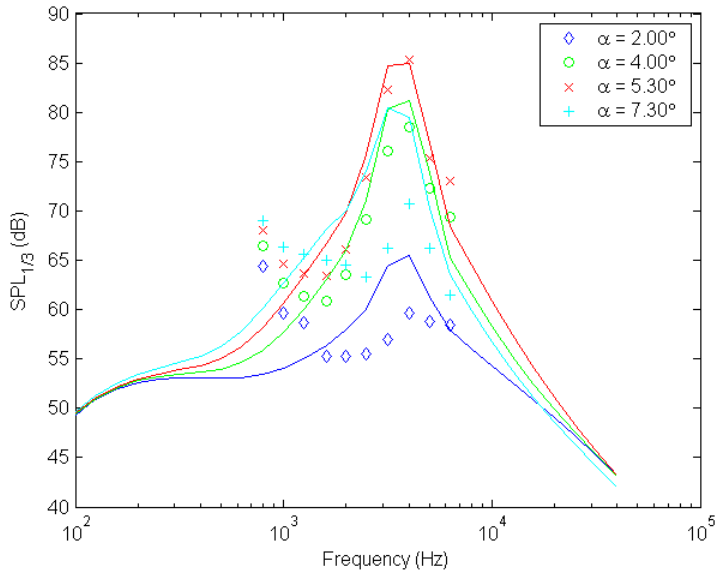

Figure 4. Comparison of two-dimensional NACA 0012 data to predictions for M = 0.207 at several angles of attack with no boundary layer tripping

could be made. The assumptions used in the prediction code are identical to those used in Figure 2. The agreement between data and predictions is reasonable and is within 3 dB for all Mach numbers, with the best agreement occurring for a Mach number of 0.163.

Figure 4 shows data and predictions for the same airfoil over a range of angles of attack at a fixed Mach number under the same tunnel conditions as Figure 2, except no boundary layer tripping. In this figure, laminar vortex shedding noise is the dominant source, as made evident by the pronounced peak near 3 kHz in each of the spectra. The agreement between data and predictions for the 4.0° and 5.3° angle of attack cases is particularly good, with less than 1 dB difference in the middle frequency range. The noise peaks for the highest and lowest angles of attack are overpredicted, with an approximately 10 dB difference at an angle of attack of 7.3°.

Figure 5 compares predictions and data for an S822 airfoil at a fixed Mach number, 0.038, over several different angles of attack. The airfoil has been "lightly" tripped (see boundary layer tripping section below) and turbulent boundary layer trailing edge noise is assumed dominant. Even though this airfoil has a significant amount of camber relative to the symmetric NACA 0012, the predicted sound pressure levels are fairly reasonable for frequencies of 3 kHz and less. Above 3 kHz, the agreement between predictions and test data decreases. As seen in Figure 2, the trends of amplitude with frequency are predicted fairly well; however, the relative differences between angles of attack are not well represented by the prediction method for these particular test conditions. One possible reason for this discrepancy is that in the prediction code, the boundary layer thickness is empirically modeled from NACA 0012 data and is, therefore, incorrectly predicted for the S822 airfoil. A possible improvement to the prediction code, that will be a focus of future work, will be a more accurate prediction method for boundary layer thickness that can incorporate differences in airfoil shape.

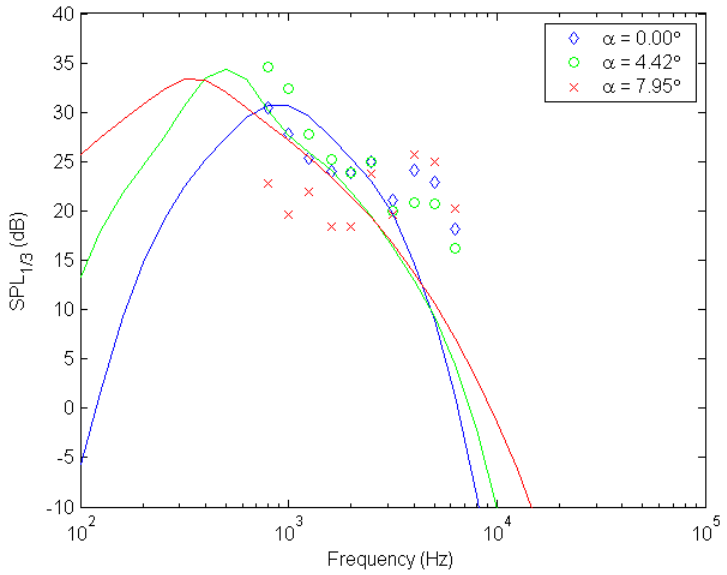

Figure 5. Comparison of two-dimensional S822 data to predictions for M = 0.038 at several angles of attack

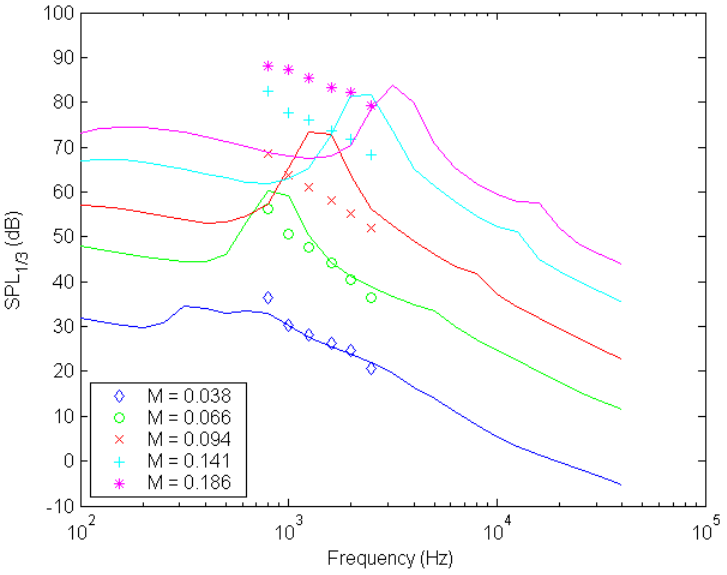

Figure 6. Comparison of two-dimensional S822 data to prediction for α = 4.42° at several Mach numbers with turbulent inflow (TI = 9%, L = 60 mm) and no boundary layer tripping

Figure 6 compares data and the predicted sound pressure levels for an S822 airfoil in a turbulent inflow at various wind tunnel Mach numbers. The Reynolds numbers for these tunnel conditions, based on chord length, were between 200,000 and 1 million. The boundary layer of the airfoil is not tripped, so in addition to trailing edge and turbulent inflow noise, laminar vortex shedding noise from the lower surface is possible. As described above, the turbulent inflow noise is a function of both the turbulence intensity and the turbulent length scale in the flow. The turbulence in the wind tunnel was created by adding a fixed-width mesh just upstream of the test

section [9]. After adding this mesh, the turbulence intensity in the center of the test section was measured as 9% by a hot-wire anemometer. Because the model was located only five mesh widths downstream of the mesh, there was insufficient distance for the turbulence to become fully isotropic. Therefore, the dominant turbulent length scale was assumed to be identical to the mesh width of 60 mm. Using these values for the parameters in the code, researchers found that the predicted sound pressure levels from the airfoil gave reasonable results for the lowest Mach numbers. Notice that there are fewer points in Figure 6 than in previous figures because it is believed that the frequencies above 3 kHz are contaminated by extraneous noise sources in the wind tunnel produced by the turbulence grid [9]. As the Mach number increases, the agreement between test data and predictions worsens. At the lower frequencies, the data are underpredicted, while the peak in the predicted spectra (primarily laminar from vortex shedding noise) overestimates the measured values. Note that at the highest Mach number, the differences between predictions and test data are as much as 10 dB. These differences may be attributed to a dependency of turbulence intensity and turbulent length scale on tunnel speed, which was not modeled.

Full-Scale Turbine

The next step in validation was to model a full-size wind turbine and compare the semi-empirical prediction to available measured data.

Researchers chose the Atlantic Orient Corporation (AOC) 15/50 turbine, operating at the National Wind Technology Center (NWTC), for validation. This three-bladed turbine has a rated power of 50 kilowatts (kW), a rotor diameter of 15 m, a hub height of 25 m, and a fixed rotational speed of 64.6 RPM (independent of mean wind speed). The trailing edge thicknesses of the blades were assumed to be 1% of the chord length, which is typical for many wind turbine designs. The turbine has tip brakes on each blade and operates downwind of the tower, both of which produce potential noise sources that are not modeled accurately in the semi-empirical code. For example, the presence of the tower upwind of the rotor plane may introduce turbulent eddies that could contribute significantly to the noise. Also, because the AOC has no nacelle, gearbox noise could potentially contribute to the farfield noise. The acoustic noise measurements of this turbine were taken according to IEC 61400-11 [12] standards, and the sound pressure levels shown in this report are from a single microphone 32.5 m downwind of the tower center at the base [13].

Correctly modeling the turbulent inflow of the atmosphere was important for accurately estimating aeroacoustic noise. The wind inputs for the predictions were created using SNWind [14], NREL's three-dimensional wind simulation code. And, for turbulent inflow noise, the turbulent length scale for all predictions (unless otherwise noted) was 61.25 m, the IEC specified length for this hub height.

Figure 7 shows the overall sound pressure level[1] (OASPL) as a function of wind speed for the AOC turbine. Two curves in the figure represent predictions of the turbine operating in turbulence level A wind conditions, as specified by the IEC standard [7], which are similar to conditions measured at the NWTC. The bottom curve represents the turbine operating in steady winds with no turbulence. The difference between the two curves with turbulence is the

[1] The overall sound pressure level (OASPL) at each wind speed is the integral of the total mean square pressure from all contributing noise sources over the frequency range of interest at the observer location.

condition of the boundary layer over the blades: tripped or not tripped. Because the turbine is relatively small, it is possible that laminar vortex shedding noise is radiated if the boundary layer is not tripped. But, because the turbine is operating in highly turbulent winds, laminar flow may not occur and the boundary layers over the blades are effectively tripped. Thus, both boundary layer conditions are modeled, because the true physical state of the boundary layer is unknown. As seen in the figure, the difference in predicted overall sound pressure levels between tripped and not tripped is no larger than 1 dB. Also, both of these predictions are fairly close to the measured test data, underpredicting the OASPL by only 2–3 dB at higher wind speeds. The predicted values using no turbulence underpredicted the measured data by 10–20 dB.

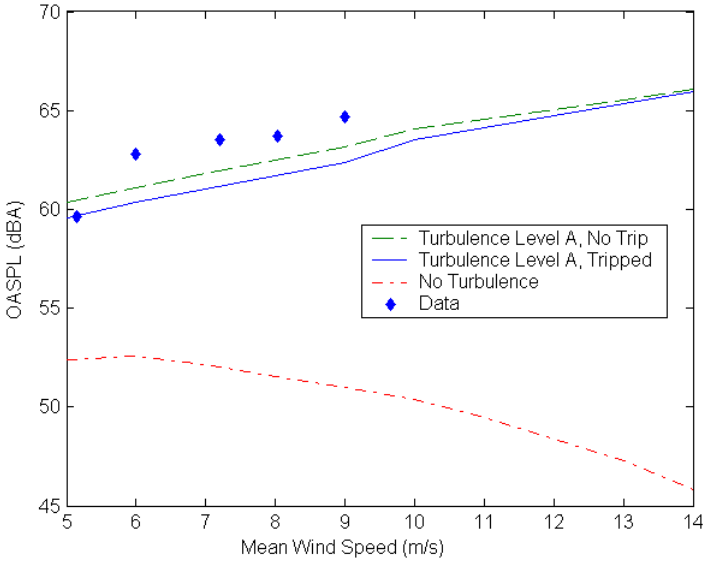

Figure 7. OASPL vs. wind speed for AOC turbine

Figure 8 breaks down the OASPL shown in Figure 7 into various components. The total OASPL in this figure is identical to the line in Figure 7 for turbulence level A and no boundary layer tripping. From the figure, it is obvious that turbulent inflow noise dominates the total noise signature of the turbine with the next loudest noise sources being the blunt trailing edge noise or laminar vortex shedding noise, depending on mean wind speed.

Figure 9 shows the predicted one-third octave band spectra of all noise sources for a mean wind speed of 8m/s along with measured test data. The turbulence intensity used to produce this figure was 22% (IEC level A), and the boundary layers over the blades were untripped so that laminar vortex shedding noise was modeled. As with the OASPL, the turbulent inflow noise dominates the total spectrum for most frequencies. In the narrow range between 1 and 2 kHz, tonal components from laminar vortex shedding and trailing edge bluntness contribute, but all other sources are at least 20 dB quieter and insignificant. Comparing to the measured test data, the predicted total noise spectrum agrees very well in the range between 1 and 5 kHz. However, the peak in the data near 800 Hz is not modeled, and the prediction overestimates the noise for frequencies below 500 Hz.

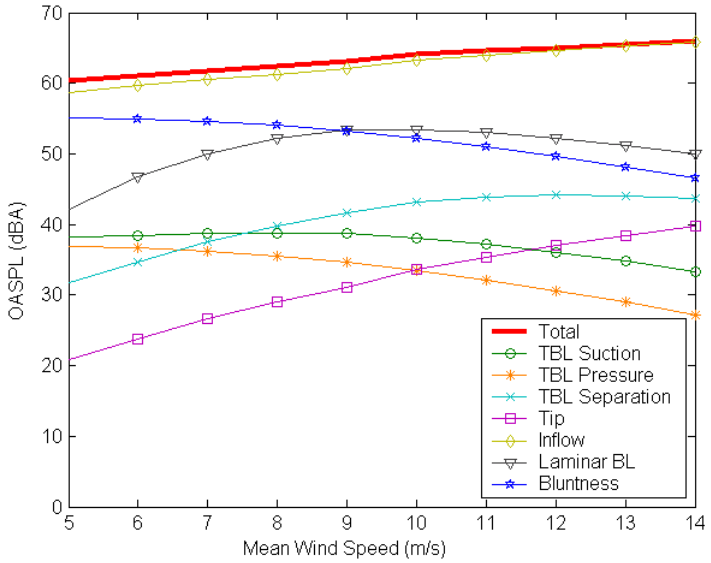

Figure 8. Components of OASPL vs. wind speed for AOC turbine

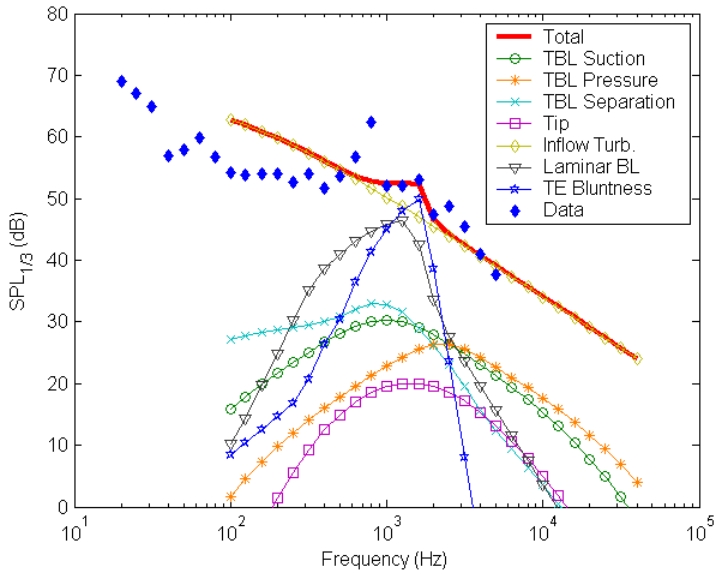

Figure 9. Components of sound pressure level vs. frequency for AOC turbine in 8m/s turbulent winds

Previous studies [15], using the identical turbulent inflow model, have shown that although turbulent inflow noise tends to dominate at lower frequencies, it also tends to have less influence than airfoil self noise at higher frequencies, unlike the trend in Figure 9. These studies were of larger turbines than the AOC, and the dominance of turbulent inflow noise at higher frequencies may be a result of its relatively small size. Further studies [16] have shown that turbulent inflow noise is secondary to airfoil self noise. This questions the validity of the turbulent inflow noise model, and further research in this area is required.

It should be noted that because the AOC is a downwind turbine, the tower shadow introduces turbulent eddies that may add significantly to the measured noise. Currently, these eddies are not modeled in the prediction code, but their influence on the measured data may explain the agreement between prediction and measurements in Figure 9, which may not occur if the AOC turbine operated upwind. Again, further research is required.

Turbulent Length Scale

Predicted turbulent inflow noise is very sensitive to the length scale of the turbulence. In previous studies [15], researchers assumed that length scales on the order of 100 m, the dominant sources of energy in the atmospheric boundary layer, were the primary contributors to turbulent inflow noise. In contrast, the work of Amiet [4] (where the empirical relations for inflow turbulence noise originated) used length scales more on the order of 1 cm. Researchers also know that, for downwind turbines, turbulent length scales on the order of the tower diameter (~1m) can be introduced. It remains unclear which length scale should be used to predict wind turbine noise and whether these length scales are independent of turbine size.

Figure 10 shows the effect of turbulence length scale on the total sound pressure level[2] radiating from the AOC wind turbine. The plot shows predictions based on an 8 m/s mean wind speed in an IEC class A turbulence field (turbulence intensity = 22%). The measured data in the plot are for similar wind conditions. For a length scale of 61.25 m (the IEC specified length), the turbulence inflow noise dominates most other noise sources, as demonstrated in Figure 9. The predicted total sound pressure level agrees well with the measured data above 1 kHz, but not below this frequency. Interestingly, the data at lower frequencies seem to match most closely to the curve using a length scale of 6.125 m, which is on the order of the rotor radius. This suggests that the rotor radius may be a more appropriate length scale in this frequency range. While the absolute levels of sound pressure level for the largest length scales are closest to the test data, the spectral peak near 1000 Hz is not accurately predicted. It is possible that this peak in the data is caused by gearbox noise, which is not represented by the code. Further study into the correct use of length scale and the turbulent inflow noise model itself should be performed.

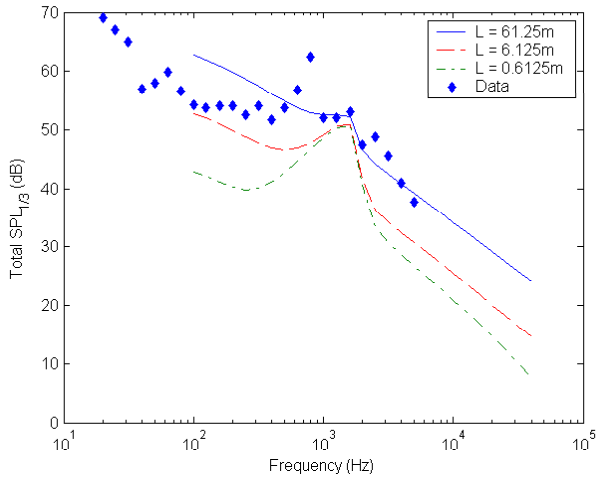

Figure 10. Effect of inflow turbulence length scale on total sound pressure level for AOC wind turbine in turbulent 8m/s winds

[2] Total sound pressure level is the sum of one-third octave band spectra from each of the six different noise sources.

Blade Pitch Angle

Figure 11 shows the effect of blade pitch angle on the total sound pressure level spectrum in a steady 8 m/s wind. Turbulent inflow noise is neglected because pitch angle has little effect on this noise source. The boundary layers over the blades are not tripped resulting in a peak from laminar vortex shedding noise between 400 Hz and 2 kHz. In the frequency ranges 100–300 Hz and 600–1000 Hz, the noise is slightly reduced by increasing the pitch angle of the blades toward feather. In the range between 300 and 600 Hz, the opposite is true. Because it is an integrated quantity, it is unclear if these changes will have any effect on the A-weighted OASPL of the turbine. For an untwisted blade, researchers expect that increasing blade pitch angle will decrease the noise produced, because the angle of attack for all airfoils is reduced.

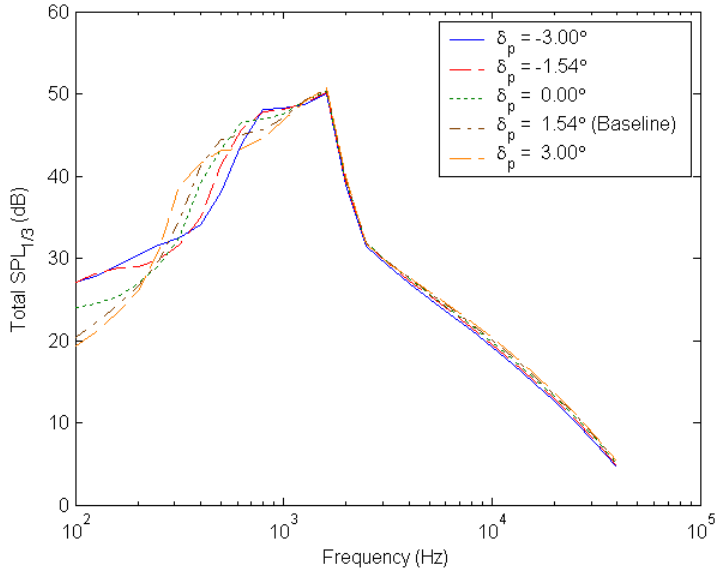

Figure 11. Effect of blade pitch angle on total sound pressure level for AOC wind turbine in steady 8 m/s winds (no turbulent inflow noise)

Boundary-Layer Tripping

In the semi-empirical code, the boundary-layer thicknesses are calculated based on two different settings for boundary-layer tripping: light or heavy. The heavy-trip boundary-layer thicknesses are based on the original measurements by Brooks, Pope, and Marcolini of a NACA 0012 [2], where grit was applied from the leading edge of the airfoil to 20% chord. This level of boundary layer tripping is unlikely to occur naturally. The light trip, considered more physically realistic, is calculated in the same manner as the heavy trip and then multiplied by a correction factor of 0.6. For the natural tripping (i.e., bugs, dirt etc.) associated with wind turbines, the light-trip setting is most likely to model the correct physics. Turbulent inflow can also cause transition in the boundary layers over the blades. Therefore, newly installed "clean" turbines operating in highly turbulent atmospheric conditions are likely to have boundary layer properties somewhere between untripped and lightly tripped.

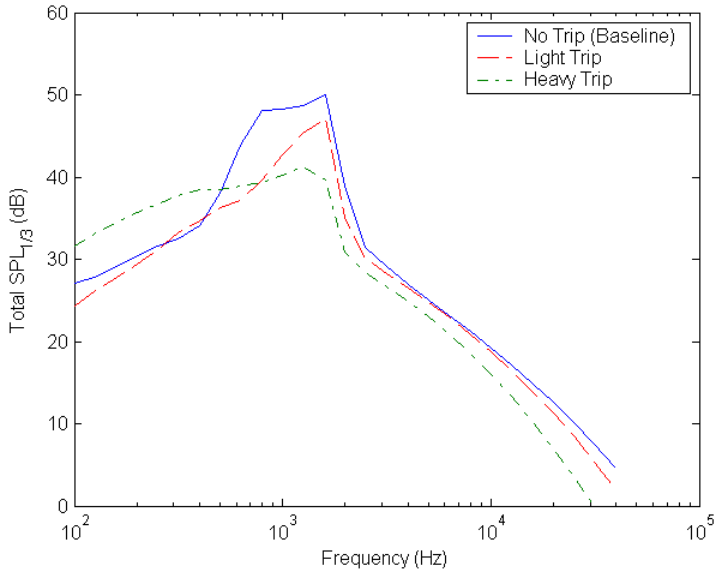

Figure 12. Effect of boundary layer tripping on total sound pressure level for AOC wind turbine in steady 8 m/s winds (no turbulent inflow noise)

Figure 12 demonstrates the effect of tripping the airfoils on the total sound pressure level spectrum. Turbulent inflow noise is neglected because it is unaffected by boundary layer properties. Adding a light trip to the turbine blades reduces the noise significantly between 400 Hz and 2 kHz. This is a result of eliminating the laminar vortex shedding noise (Figure 9). The noise levels at other frequencies remain unaffected. Adding a heavy trip decreases the noise at frequencies above 800 Hz, but adds a large amount of noise below this frequency. Notice that the tonal component from trailing edge bluntness at ~1.5 kHz is also reduced.

Trailing-Edge Bluntness

Figure 13 shows the effect of trailing-edge bluntness on the total sound pressure level radiating from the AOC turbine. In this figure, turbulent inflow noise is neglected because the bluntness has little effect on this noise source. Again, the boundary layers over the blades are not tripped, resulting in a peak from laminar vortex shedding noise between 400 Hz and 2 kHz. It is obvious

that blunt trailing edges add narrowband tones to the noise spectrum. The thickest trailing edge of 1% chord adds a large amplitude tonal peak to the spectrum around 1.5 kHz. As the thickness of the trailing edge decreases, the sound pressure level amplitude also decreases, while the frequency of the tone increases. If the trailing-edge thickness becomes infinitesimal, this noise source disappears altogether.

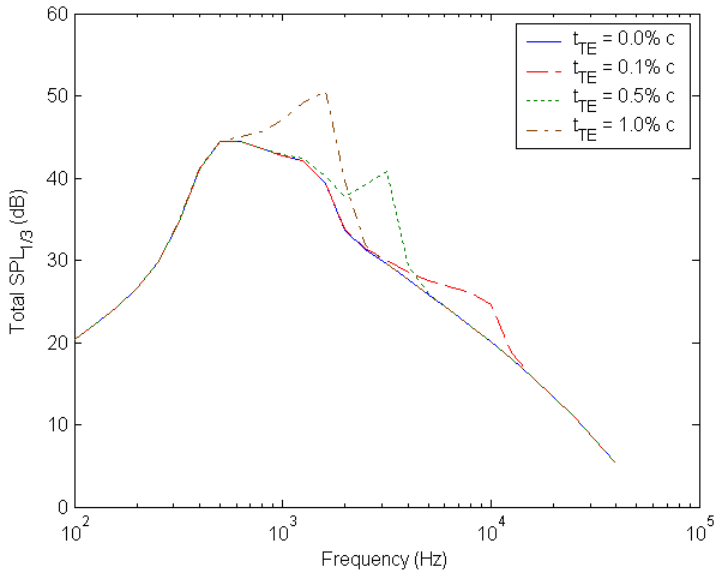

Figure 13. Effect of trailing edge bluntness on total sound pressure level for AOC wind turbine in steady 8 m/s winds (no turbulent inflow noise)

Tip Noise

As seen in Figure 9, tip noise has the least influence on the total radiated noise level from the AOC turbine. However, for other configurations, this noise source may be important, particularly at higher frequencies.

Tip noise (Figure 14) is highly dependent upon the strength of the vortex shed at the tip. Because of this, the semi-empirical code allows the user to adjust the vortex strength by modifying the effective angle of attack at the blade tip. As described in Brooks, Pope, and Marcolini [2], the multiplier for the tip angle of attack is equivalent to the ratio of the slope of the spanwise lift distribution (dL/dy) of the modeled blade to that of the blade (wing) used in their research, which consisted of an untwisted constant chord shape. Unfortunately, there is no explicit relation to determine this multiplier, although Brooks and Marcolini [17] provided additional guidance on determining this quantity for different aspect ratio blades. The more dramatic the change of lift near the tip, the stronger the vortex at the tip and the larger the multiplication factor (Figure 14). A stronger vortex directly correlates to a louder tip noise prediction. The semi-empirical code also has a switch (see Appendix) to allow for square (i.e., sharp angled) blade tips to be used instead of standard rounded tips. As seen in the figure, using square tips adds significantly to the low-frequency noise, but reduces high-frequency noise.

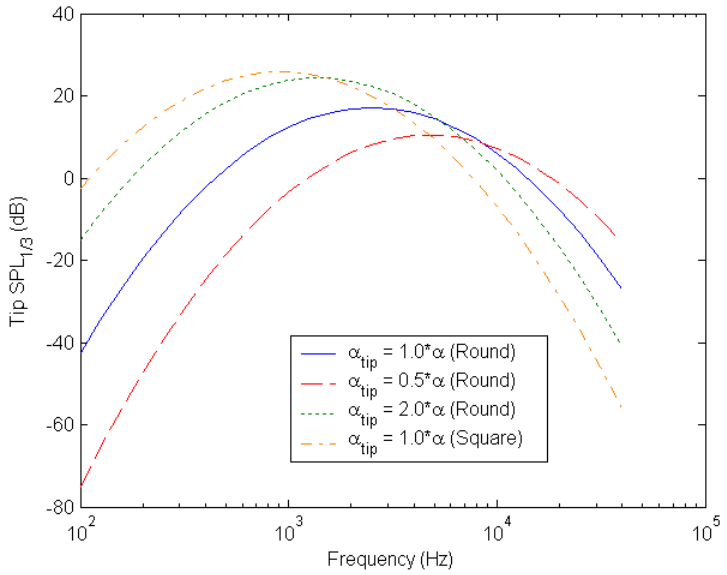

Figure 14. Effect of tip vortex strength and tip shape on tip sound pressure level for AOC wind turbine in steady 8 m/s winds (tip noise only)

Rotor Speed

Figures 15 and 16 are intended to show that the effect of turbine rotor speed on total sound-pressure level is highly dependent on the dominant noise sources. The boundary layers over the blades are not tripped in either of these figures, so laminar vortex shedding noise is modeled.

If turbulent inflow noise is included, the sound intensity appears to scale with rotor speed to the fourth power (12 dB difference by doubling speed) as shown in Figure 15.[3] If turbulent inflow noise is neglected, as in Figure 16, the response is more complex because of the interaction of several different noise sources. The dominant effects are the three forms of trailing edge noise: laminar vortex shedding, trailing edge bluntness, and turbulent boundary layer noise, for which intensity will all scale with rotor speed to the fifth power (15 dB difference by doubling speed). However, the frequencies of the noise disturbances change nonlinearly, which prevents direct scaling from one spectrum to the next.

[3] Notice also that the tonal component from trailing edge bluntness noise increases in amplitude and frequency with rotor RPM.

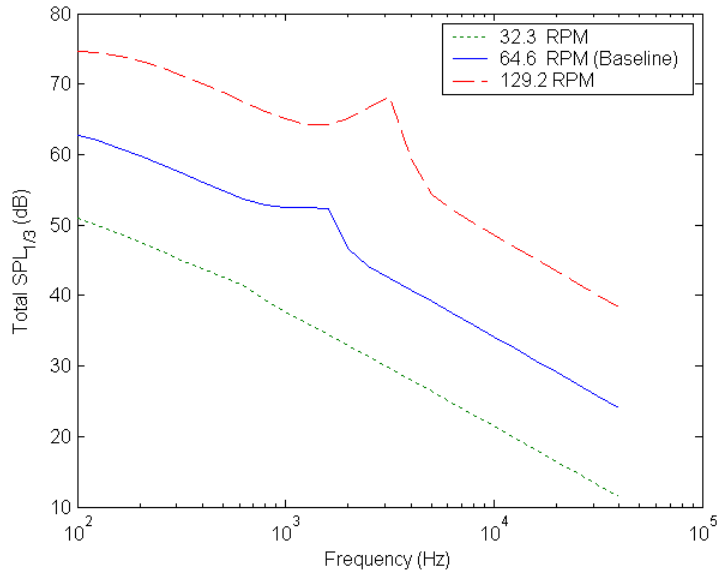

Figure 15. Effect of rotor speed on total sound pressure level for AOC wind turbine in turbulent 8 m/s winds (with turbulent inflow noise)

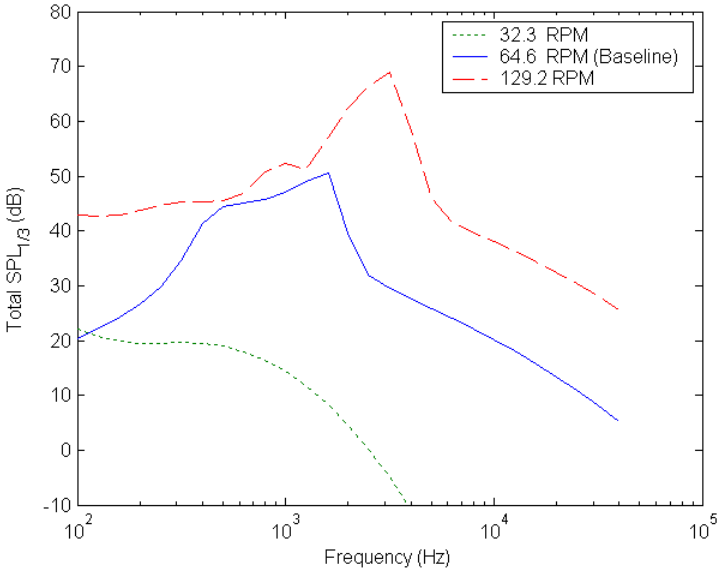

Figure 16. Effect of rotor speed on total sound pressure level for AOC wind turbine in steady 8 m/s winds (no turbulent inflow noise)

Directivity

Figure 17 shows the OASPL footprint for the AOC turbine operating in steady 8 m/s winds. Note that because the winds are steady, there is no inflow turbulence noise present in these results. The boundary layers over the blades are also untripped, so laminar vortex shedding noise is modeled. As expected, the noise levels in the rotor plane are the lowest because of the directivity of the noise radiating from the blades set at 1.54° pitch angle. The cardioid shape is typical of dipole noise sources, such as those produced near the trailing edge. Note the noise is fairly symmetric upwind and downwind of the rotor plane. This symmetry is caused by the semi-empirical relations, which are based on measurements [2] that were made above the upper surface of a symmetric airfoil. No similar measurements were made below the lower surface. Therefore, it was assumed that the noise radiating on both sides of the airfoil is equivalent. Although this assumption may be valid for trailing-edge bluntness and turbulent-inflow noise, it will introduce some error in separating flow and laminar boundary layer vortex shedding noise, which tend to radiate more from one side of the airfoil than the other.

Figure 18 is a slice through the contour of Figure 17 for OASPL as a function of distance downwind of the tower centerline at a lateral position of 0 m. Near the rotor plane, the sound pressure is lowest, but then peaks about 15 m downstream. By doubling the distance downstream (e.g., from 30 to 60 m), the OASPL is reduced by approximately 4 dB. This is less than the 6 dB decrease expected from the behavior of a pure point-source model and is a result of various constant factors in Equations 2-10.

Figure 19 provides some insight into the distribution of the noise sources in the rotor plane. This figure represents the average distribution of noise sources that contribute to the total sound pressure level, as observed 32.5 m upwind of the tower centerline at hub height. The average

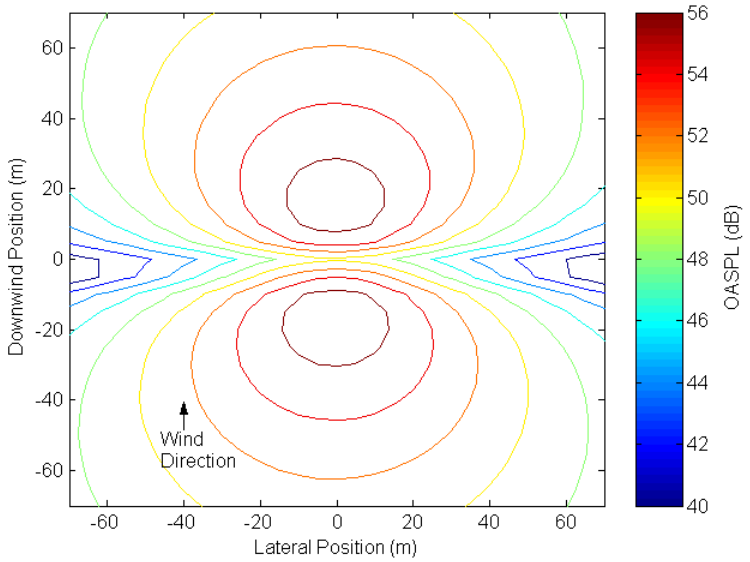

Figure 17. OASPL noise footprint for AOC turbine in steady 8 m/s winds (no turbulent inflow noise)

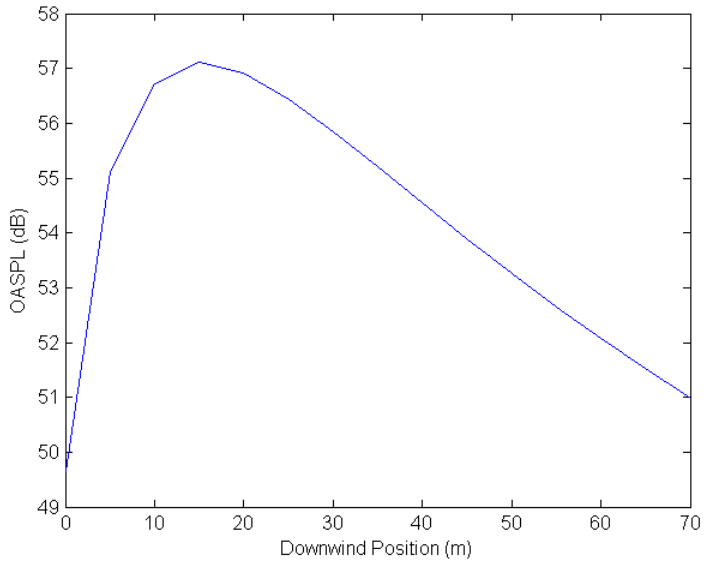

Figure 18. OASPL as a function of downwind distance for AOC turbine in steady 8 m/s winds (no turbulent inflow noise)

levels were obtained from a 5-minute simulation of the AOC turbine operating in steady 8 m/s winds. As expected, the sound pressure level of the source distribution increases along the span of the blades because of a linear increase in velocity. Because the observer position is at hub height, the apparent source distribution is fairly symmetric. The source amplitude on the top of the rotor is slightly higher than that on the bottom because of the mean wind speed gradient across the rotor plane, although the total velocity between the top and bottom is less than 1%.

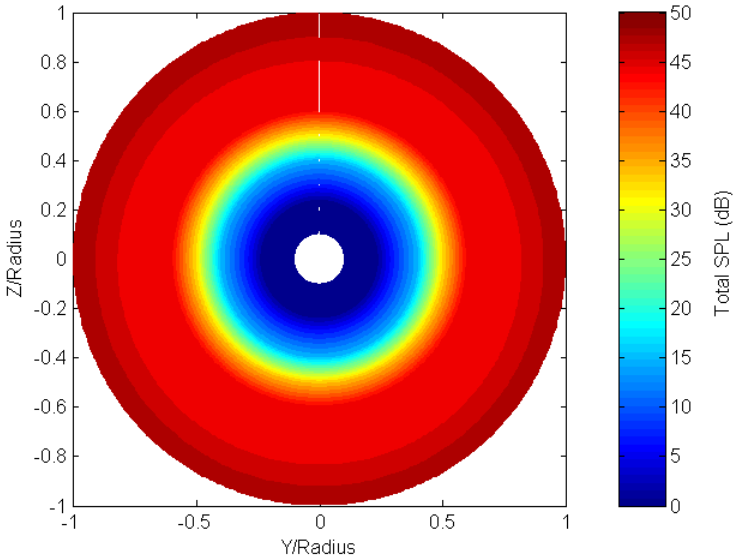

Figure 19. Total sound pressure level across rotor of AOC as measured from hub height in steady 8 m/s winds (no turbulent inflow noise, untripped boundary layers)

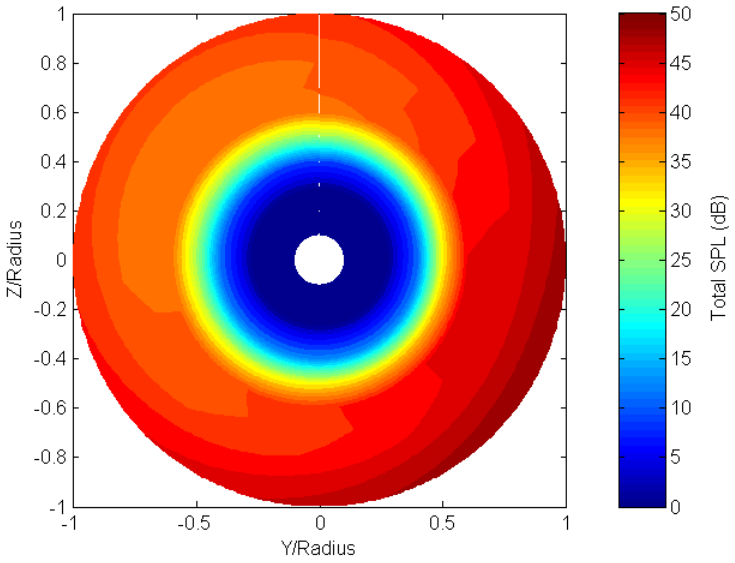

Figure 20. Total sound pressure level across rotor of AOC as measured from ground observer in steady 8 m/s winds (no turbulent inflow noise, untripped boundary layers)

Figure 20 shows the distribution of apparent noise sources for the AOC operating in the same conditions, as perceived by an observer 32.5 m upwind at ground level. From this observer position, the source distribution is not symmetric as in Figure 19. The loudest portions of the rotor are in the lower right-hand portions of the rotor plane. This effect is a result of Doppler amplification of the perceived sound pressure level at these locations, as specified by Equations 11 and 12. The turbine turns clockwise as seen from upwind[4] and, therefore, moves toward the observer on the right half of the rotor plane and away from the observer on the left. Doppler amplification increases the observed sound pressure level for sources moving toward the observer and decreases the sound pressure level for those moving away.

Conclusions

A series of semi-empirical acoustic noise prediction subroutines was written and incorporated into NREL's aeroelastic simulation code, FAST. The subroutines were used to predict relative amplitudes and trends of sound pressure level data from acoustic tests of two-dimensional airfoils and a full-size wind turbine. Prediction accuracy of the absolute sound pressure level for the two-dimensional airfoil data was dependent on wind tunnel test conditions and the airfoil model. The best predictions were made using a NACA 0012 model at moderate angle of attack with a laminar boundary layer. Predictions of the acoustic emission from the full-size turbine studied (AOC 15/50) were dominated by turbulent inflow noise. The next-loudest noise sources were trailing-edge bluntness and laminar vortex shedding. There is some uncertainty as to the absolute accuracy of the turbulent inflow model and what turbulent length scale should be used in the model. Comparison of the prediction to data demonstrates that the length scale should be smaller than that specified by the IEC standard for certain frequency ranges. Further study of this issue should be performed using additional data and several different-sized wind turbines. The total sound pressure level amplitude of a full-turbine model was found to be most sensitive to

[4]The sign of the y coordinate in figures 19 and 20 is opposite to the tower coordinate system used in the input file described in the appendix.

rotor speed. Thick trailing edges on wind-turbine blades introduce large amplitude tonal noise sources into the noise spectrum that can add significant noise at certain frequencies. The directivity of the total sound pressure level was dominated by the dipole behavior of the trailing-edge noise. Doppler amplification creates a skewed map of the apparent source distribution across the rotor plane for an observer on the ground.

Further improvements to the semi-empirical code will include updating current modules with more accurate physical models and adding completely new modules that model physics. The next version of the code will attempt to include a routine to more accurately calculate turbulent inflow noise and another to more accurately predict boundary layer thickness. This will allow users to model different airfoil shapes for their turbines. New modules that will be added include tower interaction and atmospheric propagation models. As researchers continue to develop the code, it will be validated using data from concurrent wind tunnel testing and computational aeroacoustic efforts, as well as measurements of larger turbines that have been studied more extensively in the literature.

References

[1] Buhl, M. L.; Jonkman, J. M.; Wright, A. D.; Wilson, R. E.; Walker, S. N.; Heh, P. 2002. *FAST User's Guide*. NREL/EL-500-29798, National Renewable Energy Laboratory: Golden, CO.

[2] Brooks, T. F.; Pope, D. S.; Marcolini, M. A. 1989. "Airfoil Self-Noise and Prediction." *NASA Reference Publication 1218*, National Aeronautics and Space Administration, USA.

[3] Lowson, M. V. 1992. "Assessment and Prediction of Wind Turbine Noise." Flow Solutions Report 92/19, ETSU W/13/00284/REP Bristol, England.

[4] Amiet, R. K. 1975. "Acoustic Radiation from an Airfoil in a Turbulent Stream" *Journal of Sound Vibration* (41:4), pp. 407-420.

[5] Ffowcs-Williams, J. E.; Hall, L. H. 1970. "Aerodynamic Sound Generation by Turbulent Flow in the Vicinity of a Scattering Half-Plane." *Journal of Fluid Mechanics* (40:4), pp. 657-670.

[6] Schlichting H. 1979. *Boundary-Layer Theory*, 7th Edition. McGraw-Hill, New York: NY.

[7] Wagner, S.; Bareiss, R.; Guidati, G. 1996. *Wind Turbine Noise*. Springer-Verlag, New York: NY.

[8] IEC/TC88. 1998. 61400-1 ed. 2. *Wind turbine generator systems-part 1: Safety Requirements*. International Electrotechnical Commission (IEC).

[9] Oerlemans, S. Publication pending. *Wind Tunnel Aeroacoustic Tests of Six Airfoils for Use on Small Wind Turbines*. National Aerospace Laboratory, Emmeloord, The Netherlands. NREL SR-500-34470. National Renewable Energy Laboratory: Golden, CO.

[10] Sijtsma, P. 2002. "Calculating Absolute Source Powers from Phased Arrady Measurements." NLR-CR-2002-358, National Aerospace Laboratory, Emmeloord, The Netherlands.

[11] Tangler, J. L.; Somers, D. M. 1995. "NREL Airfoil Families for HAWTs." *WindPower 1995 Proceedings*, American Wind Energy Association, Washington, D.C.

[12] IEC/TC88. 1998. 61400-11 *Wind turbine generator systems-part 11: Acoustic Noise Measurement Techniques*, 88/67/FDIS. International Electrotechnical Commission (IEC).

[13] Huskey, A.; Link, H. F.; Butterfield, C. P. 1999. *Wind Turbine Generator System Acoustic Noise Test Report for the AOC 15/50 Wind Turbine*. AOC1550-C-A-99182-1000, National Renewable Energy Laboratory, Golden, CO.

[14] Kelley, N. D. 1993. "Full Vector (3-D) Simulation in Natural and Wind Farm Environments Using an Expanded Version of the SNLWIND (Veers) Turbulence Code." *Wind Energy 1993*, S.M. Hock (ed.), SED-Vol.14, ASME.

[15] Fuglsang, P.; Madsen, H. A. 1996. *Implementation and Verification of an Aeroacoustic Noise Prediction Model for Wind Turbines*. Riso-R-867(EN), Riso National Laboratory, Roskilde, Denmark.

[16] Fuglsang, P.; Guidati F. 2003. Personal Communication.

[17] Brooks, T. F.; Marcolini, M. A. 1986. "Airfoil Tip Vortex Formation Noise." *AIAA Journal* (24:2), pp. 246-252.

[18] Laino, D. J.; Hanson, A. C. 2002. *User's Guide to the Wind Turbine Aerodynamics Computer Software AeroDyn*. Windward Engineering, Salt Lake City: UT.

Appendix: Code Operation

Before running the semi-empirical noise-prediction code, the user should become familiar with the FAST aeroelastic simulation code in which the aeroacoustic code is embedded [1]. This code has its own set of input files that describe many turbine parameters. The main FAST input file must be modified in order for the noise-prediction subroutines to be called, which is described below. It is also recommended that the user learn about the SNWind code [14], which can be used to create turbulent wind input files for FAST.

Input Files

To use the noise-prediction code, a noise-input file must be created, and the input file for FAST [1] must be slightly modified.

Figure 21 shows the three additional lines that must be inserted in the FAST input file. The first line is added to the "features switches" section of the FAST input file and contains the variable *CompNoise*. This variable is either true or false depending on whether or not the user would like to compute the aerodynamic noise. Two additional lines must be inserted between the "aerodyn" and "output" sections. These lines are skipped if *CompNoise* is false. The first line is a comment that marks the beginning of the "noise" section of the FAST file, and the second line contains the variable *NoiseFile*, which is the location of the noise input file used by FAST.

Figure 22 shows the input file specified by the variable *NoiseFile*. Note that the first 19 lines of this input file must have the format shown below, including blank lines, in order for the file to be read correctly. The first two lines of input file can be used for comments. The third line of input file is the speed of sound measured in meters per second. The next line is the variable *ALPRAT*, which is a multiplier for the angle of attack of the tip airfoil. This multiplier is only used in the calculation of tip noise and has a default value of 1.0. A value higher than 1.0 is indicative of a highly loaded tip that may result from spanwise twist or blade taper. The next line of the input file is the variable *ROUND*, which is true for a rounded blade tip or false for a square-edged blade tip. The next section of input lines are switches to determine what sources of noise are to be computed. The values for the switches should be set to 0 if the noise source should NOT be computed and 1 if the noise source should be computed (with the exception of *ITRIP*).

```
...
True        CompAero   - Compute aerodynamic forces (switch)
True        CompNoise  - Calculate aerodynamic noise (switch)
---------------------- INITIAL CONDITIONS -------------------------------------
...
---------------------- AERODYN ------------------------------------------------
"D:\acoustics\AeroDyn.ipt" ADFile  - Name of file containing AeroDyn input parameters
---------------------- NOISE --------------------------------------------------
"D:\acoustics\Noise.ipt" NoiseFile  - Name of file containing noise input parameters
---------------------- OUTPUT -------------------------------------------------
False        SumPrint    - Print summary data to "<RootName>.fsm" (switch)
...
```

Figure 21. Sample modified FAST input file

The switches in the input file should appear in the following order: *IBLUNT* for trailing-edge bluntness noise, *ILAM* for laminar boundary-layer noise (note, if *ITRIP* is any value other than 0, *ILAM* is automatically set to 0), *ITIP* for tip noise, *ITRIP* to trip the boundary layer, *ITURB* for turbulent boundary-layer trailing-edge noise, and *IInflow* for turbulent inflow noise (i.e., leading-edge noise). *ITRIP* can have a value of 0, for no boundary layer trip, or 1 for a "heavy" trip [2], or 2 for a "light" trip. The value of two is most likely for "naturally" tripped boundary layers on wind turbines (i.e., from bugs, surface defects, etc.).

The next input line is the variable *NoiseOutSwitch* that determines the OASPL for each blade element that is output to the file with the extension ".spl" (see below). The values of *NoiseOutSwitch* for various noise sources are listed in Table 1. The next line of input contains the coordinates of the observer location (x, y, z) relative to the center of the tower-base in the tower-base coordinate system of FAST [1] (in meters). The coordinate x is the upwind/downwind distance, where a negative value indicates an upwind observation point. The y coordinate is the lateral distance from the tower centerline (positive left, looking downwind), and the z coordinate is the vertical distance from the tower base (positive upward).

The final lines of the noise-input file contain two columns, the first being the thickness of the trailing edge (in meters) and the second being the solid angle between the upper and lower surface at the trailing edge (in degrees). These two parameters are used exclusively to calculate blunt trailing-edge noise. Note that in the figure that there are several rows of inputs, where each row represents a blade airfoil element identical to those specified in the Aerodyn input file [18], the aerodynamic module of FAST. The number of elements listed in this file must be identical to those of the Aerodyn file. Also, because there is only one table of input data, all blades on the wind turbine are assumed to have identical trailing-edge properties.

```
Input file for aeroacoustic code

344.05         C0                SPEED OF SOUND                      METERS/SEC
1.0            ALPRAT            TIP SPANWISE LIFT CURVE SLOPE (Default = 1.0)   ---
.TRUE.         ROUND             LOGICAL INDICATING ROUNDED TIP     ---

0       IBLUNT             FLAG TO COMPUTE BLUNTNESS NOISE    ---
0       ILAM               FLAG TO COMPUTE LBL NOISE          ---
1       ITIP               FLAG TO COMPUTE TIP NOISE          ---
2       ITRIP              FLAG TO TRIP BOUNDARY LAYER (=0 no trip, =1 heavy trip, =2 light trip)
1       ITURB              FLAG TO COMPUTE TBLTE NOISE        ---
1       IInflow            FLAG TO COMPUTE Turbulent Inflow NOISE        ---

1       NoiseOutSwitch     Switch to determine which time series of sound pressure level output

50.00   70.00   0.000     (x,y,z) Observer location in tower-base coordinate system (m)

Thickness (m)    PSI (deg)    Same elements as aerodyn inputs
      0.00       12.5
      0.00       12.5
      0.00       12.5
      0.00       12.5
      0.00       12.5
      0.00       12.5
      0.00       12.5
      0.00       12.5
      0.00       12.5
      0.00       12.5

C       Thickness          SEGMENT TRAILING EDGE THICKNESS    METERS
C       PSI                SEGMENT BLUNTNESS ANGLE            DEGREES
```

Figure 22. Sample noise input file

Table 1. *NoiseOutSwitch* Values and Resulting Output

NoiseOutSwitch	Noise Mechanism
1	Total OASPL
2	Laminar boundary layer OASPL
3	Total turbulent boundary layer OASPL (combination of 7,8 and 9)
4	Inflow turbulence OASPL
5	Tip vortex OASPL (tip elements only)
6	Blunt trailing-edge OASPL
7	Turbulent boundary layer OASPL from pressure side of airfoil
8	Turbulent boundary layer OASPL from suction side of airfoil
9	Separating flow OASPL

Output files

Besides the regular output files of FAST, the acoustic-noise subroutines produce two additional files with the extensions ".spl" and ".nos." The .spl file, partially shown in Figure 23, contains the time-series information of the calculated sound pressure level specified by *NoiseOutSwitch* for each blade element, as well as the azimuth angle (in degrees). Data in this file can be used to examine the time history of the noise and also to calculate azimuth averaged sound pressure levels, such as those seen in figures 19 and 20. This output file begins at the time specified by the variable *TStart* in the FAST input file.

```
These predictions were generated by FAST (v4.03, 15-Jan-2003) on 04-Jun-2003 at 17:37:10.
The aerodynamic calculations were made by AeroDyn (12.52, 28-Mar-2003).

AOC FAST model for noise code validation

Total Overall Sound Pressure Level (dB)

   Time   Azimuth      Bl1-Elem 1     Bl1-Elem 2     Bl1-Elem 3     Bl1-Elem 4
 10.000  275.997         34.727         40.796         45.691         49.762
 10.005  277.935         34.708         40.784         45.674         49.736
 10.010  279.873         34.818         40.862         45.714         49.748
 10.015  281.811         34.923         40.937         45.753         49.761
 10.020  283.749         34.891         40.902         45.713         49.716
 10.025  285.687         35.120         41.079         45.827         49.787
 10.030  287.625         35.213         41.147         45.863         49.800
 10.035  289.563         35.305         41.213         45.898         49.813
 10.040  291.501         35.394         41.276         45.931         49.825
 10.045  293.439         35.480         41.338         45.963         49.837
 10.050  295.377         35.564         41.397         45.993         49.848
 10.055  297.315         35.645         41.454         46.021         49.857
 10.060  299.253         35.608         41.418         45.982         49.815
 10.065  301.191         35.682         41.480         46.020         49.835
 10.070  303.129         35.699         41.492         46.019         49.824
 10.075  305.066         35.716         41.504         46.018         49.813
 10.080  307.005         35.733         41.515         46.017         49.802
 10.085  308.943         35.748         41.526         46.015         49.792
 10.090  310.880         35.763         41.536         46.013         49.781
 10.095  312.819         35.776         41.545         46.011         49.771
 10.100  314.757         35.736         41.509         45.974         49.733
 10.105  316.694         35.799         41.560         46.005         49.749
 10.110  318.633         35.719         41.503         45.957         49.706
...
```

Figure 23. Sample .spl output file

The second output file with the extension .nos, seen in figures 24 and 25, contains all of the input information for the noise code and also the time averaged spectra for the individual acoustic noise sources, along with a total noise spectrum, given in units of dB. These spectra are obtained by time averaging the mean square pressures of the noise sources for each third octave frequency band and then converting them into sound pressure levels. As with .spl the file, the averaging process does not start until after the value of *TStart* is passed. This allows the user to prevent any startup transients in the simulation from contaminating the average spectral values.

```
These predictions were generated by FAST (v4.03, 15-Jan-2003) on 04-Jun-2003 at
The aerodynamic calculations were made by AeroDyn (12.52, 28-Mar-2003).

 AOC FAST model for noise code validation


10  NUMBER OF SEGMENTS              ---
344.0500      SPEED OF SOUND        METERS/SEC
1.46390E-05   KINEMATIC VISCOSITY   M2/SEC
1.000000      TIP LIFT CURVE SLOPE  ---
T  LOGICAL INDICATING ROUNDED TIP   ---

 F  FLAG TO COMPUTE BLUNTNESS NOISE ---
 F  FLAG TO COMPUTE LBL NOISE       ---
 T  FLAG TO COMPUTE TIP NOISE       ---
 2  FLAG TO TRIP BOUNDARY LAYER     ---
 T  FLAG TO COMPUTE TBLTE NOISE     ---
 T  FLAG TO COMPUTE Turbulent Inflow NOISE     ---

 Mean Wind Speed =    8.092841     m/s
 Turbulence Intensity =    21.33508     %

  -32.50000      0.0000000E+00  0.0000000E+00
 Observer location relative to tower base centerline

 Segment#      C       L       H           PSI
         1    0.494    0.470    0.005   12.500
         2    0.579    0.748    0.006   12.500
         3    0.680    0.752    0.007   12.500
         4    0.744    0.748    0.007   12.500
         5    0.738    0.752    0.007   12.500
         6    0.677    0.740    0.007   12.500
         7    0.616    0.760    0.006   12.500
         8    0.558    0.740    0.006   12.500
         9    0.497    0.760    0.005   12.500
        10    0.436    0.740    0.004   12.500

                                                ONE-THIRD OCTAVE
                                              SOUND PRESSURE LEVELS


                     PRESSURE        SUCTION      SEPARATION
     FREQUENCY(HZ)    SIDE TBL       SIDE TBL       SIDE TBL        LAMINAR

    -------------- -------------- -------------- -------------- --------------

        100.000          8.596         20.990         29.807          0.000
        125.000         11.054         22.805         30.225          0.000
        160.000         13.550         24.701         30.622          0.000
        200.000         15.629         26.338         31.012          0.000
        250.000         17.562         27.915         31.547          0.000
        315.000         19.436         29.451         32.352          0.000
        400.000         21.260         30.804         33.430          0.000
        500.000         22.886         31.682         34.381          0.000
        630.000         24.508         32.058         34.726          0.000
        800.000         26.107         31.850         33.756          0.000
       1000.000         27.440         31.156         31.612          0.000
...
```

Figure 24. Sample .nos output file (first four columns of spectrum)

```
  BLUNTNESS          TIP          INFLOW         TOTAL

 -------------- -------------- -------------- --------------

      0.000        -14.434         66.435         66.435
      0.000         -8.739         66.240         66.241
      0.000         -3.052         65.871         65.871
      0.000          1.539         65.424         65.425
      0.000          5.610         64.892         64.892
      0.000          9.282         64.264         64.265
      0.000         12.502         63.547         63.548
      0.000         14.984         62.825         62.828
      0.000         17.027         62.032         62.038
      0.000         18.581         61.173         61.180
      0.000         19.529         60.339         60.344
...
```

Figure 25. Sample .nos output file (last four columns of spectrum)

REPORT DOCUMENTATION PAGE

Form Approved
OMB NO. 0704-0188

1. AGENCY USE ONLY (Leave blank)	2. REPORT DATE	3. REPORT TYPE AND DATES COVERED
	December 2003	Technical Report

4. TITLE AND SUBTITLE	5. FUNDING NUMBERS
Semi-Empirical Aeroacoustic Noise Prediction Code for Wind Turbines	WER3.1830
6. AUTHOR(S)	
P. Moriarty and P. Migliore	

7. PERFORMING ORGANIZATION NAME(S) AND ADDRESS(ES)	8. PERFORMING ORGANIZATION REPORT NUMBER
National Renewable Energy Laboratory 1617 Cole Blvd. Golden, CO 80401-3393	NREL/TP-500-34478

9. SPONSORING/MONITORING AGENCY NAME(S) AND ADDRESS(ES)	10. SPONSORING/MONITORING AGENCY REPORT NUMBER

11. SUPPLEMENTARY NOTES

12a. DISTRIBUTION/AVAILABILITY STATEMENT	12b. DISTRIBUTION CODE
National Technical Information Service U.S. Department of Commerce 5285 Port Royal Road Springfield, VA 22161	

13. ABSTRACT *(Maximum 200 words)*

A series of semi-empirical aeroacoustic noise prediction subroutines was written and incorporated into the National Renewable Energy Laboratory's (NREL's) aeroelastic simulation code: FAST. The subroutines predict six different forms of aerodynamically produced noise that were superimposed to calculate the total aeroacoustic signature of an operating wind turbine. This report explains how the code was written, what validation against test data was performed, and how a user can implement the code to predict noise for any given turbine design.

14. SUBJECT TERMS	15. NUMBER OF PAGES
Wind turbine; noise; aeroacoustic simulation code; FAST; wind energy	16. PRICE CODE

17. SECURITY CLASSIFICATION OF REPORT	18. SECURITY CLASSIFICATION OF THIS PAGE	19. SECURITY CLASSIFICATION OF ABSTRACT	20. LIMITATION OF ABSTRACT
Unclassified	Unclassified	Unclassified	UL